Equation of state and the nucleon optical potential with three-body forces

Syed Rafi,[1] Manjari Sharma,[1] Dipti Pachouri,[1] W. Haider,[1] and Y. K. Gambhir[2,3]
[1]*Department of Physics, AMU, Aligarh, India*
[2]*Manipal University, Manipal 576104, Karnataka, India*
[3]*Department of Physics, IIT-Bombay, Powai, Mumbai 400076, India*
(Received 6 September 2012; revised manuscript received 16 December 2012; published 14 January 2013)

We report microscopic calculations of the equation of state of symmetric nuclear matter and the nucleon-nucleus optical potential in the Brueckner-Hartree-Fock approach. The calculations use several internucleon (NN) potentials, such as the Hamada-Johnston, Urbana v14, Argonne v14, Argonne v18, Reid93, and Nijm II along with and without two types of three-body forces (TBFs): the Urbana IX model and the phenomenological density-dependent three-nucleon interaction model of Lagris and Pandharipande [Nucl. Phys. A **359**, 349 (1981)] and Friedman and Pandharipande [Nucl. Phys. A **361**, 502 (1981)]. The inclusion of TBFs helps to reproduce the saturation properties for symmetric nuclear matter rather well as expected. The proton-nucleus optical potential has been calculated by folding the calculated reaction matrices (with and without three-body forces) over the nucleon density distributions obtained from the relativistic mean-field theory. The results show that the inclusion of TBFs reduces the strength of the central part of the optical potential in the nuclear interior and affects the calculated spin-orbit potential only marginally. As a test of the calculated potential, we have analyzed proton differential elastic scattering, analyzing power, and spin-rotation data from ^{40}Ca and ^{208}Pb at 65 and 200 MeV. It is observed that the inclusion of TBFs improves the agreement with the experiment especially for the polarization data.

DOI: 10.1103/PhysRevC.87.014003 PACS number(s): 21.65.Mn, 21.65.Cd, 25.40.Cm, 24.10.Ht

I. INTRODUCTION

The properties of symmetric nuclear matter (SNM) and pure neutron matter are of great importance in the development of the nuclear many-body problem with an application to nuclear as well as astrophysics. Over the past several decades, different approaches, e.g., the Brueckner-Hartree-Fock (BHF) [1], variational [2,3], Monte Carlo technique [4,5], self-consistent Green's function method [6], etc., have been developed to address the problem. The only input required in these calculations is the realistic nucleon-nucleon interaction. As a result of the importance of the equation of state (EOS), almost all internucleon potentials have been tested for their prediction of EOSs in different many-body theories. An appropriate EOS must predict the correct saturation point for SNM and must give symmetry energy compatible with phenomenology and values of compressibility in agreement with empirical estimates. It is now well established that no nonrelativistic approach, which uses only two forces, is able to predict the empirical values of the saturation properties of SNM. The major discrepancy in the predicted EOS is at densities around and higher than the saturation density. Furthermore, in the BHF approach, it has been shown [7] that, with a continuous choice, the hole-line expansion with only two-body forces converges rapidly in lowest order, and hence, there is no hope that the inclusion of higher-order terms would improve the predictions of saturation properties. In view of this, three-body forces (TBFs) have been proposed (included mostly phenomenologically) as a savior [8–10]. The inclusion of TBFs helps to achieve the nuclear saturation properties close to their empirical estimates and the desired stiffer EOS.

In the present paper, we have used the BHF approach to calculate the EOS for symmetric nuclear matter and the proton-nucleus optical potential by using several two-body and TBFs. Specifically, we have used the old hard-core Hamada-Johnston (HJ) [11], the soft-core Urbana v14 (UV14) [12], Argonne v14 (AV14) [13], Argonne v18 (AV18) [14], Reid93, and Nijm II [15] internucleon potentials with and without the three-nucleon force models (Urbana IX (UV IX) [4] and the three-nucleon interaction (TNI) model [16,17]) in BHF. The old HJ internucleon potential is used only to show that the use of a hard-core interaction underestimates the binding energy in agreement with the earlier results from Bethe and others [18,19].

We find that no two-body interaction, considered in the present paper, is able to reproduce the empirical saturation property of SNM in agreement with earlier findings [8–10]. Our results show that the use of the UV IX and TNI models of three-body forces with UV14, AV14, and AV18 brings the saturation point closer to the empirical values. The results for the EOS show that the major effect of TBFs is to reduce attraction at higher densities. In view of this, the nuclear potential for scattering from finite nuclei calculated in BHF by using the folding model [20,21] is expected to be affected in the nuclear interior due to the inclusion of three-body forces. To investigate this, we have calculated the optical potential for the scattering of 65- and 200-MeV protons from ^{40}Ca and ^{208}Pb with and without TBFs along with AV18. We find that the use of three-body forces reduces the central potential significantly in the nuclear interior, whereas, there is a marginal effect on the spin-orbit part of the calculated optical potential at both low and high energies and for the two targets considered in the present paper. Analysis of the elastic differential cross section, polarization, and spin-rotation data, which use the calculated potential with TBFs, shows marginal improvement in agreement.

In Sec. II, we briefly present our method of calculation by using BHF. Section III presents the results and discussion, which concern the EOS, nuclear optical potential, and analysis of experimental scattering data. The conclusions are given in Sec. IV.

II. METHOD OF CALCULATION

The basic ingredient in BHF is the reaction matrix G, which satisfies the following Bethe-Goldstone equation:

$$G[\omega;\rho] = V + \sum_{k_a k_b} V \frac{|k_a k_b\rangle\ Q\ \langle k_a k_b|}{\omega - e(k_a) - e(k_b) + i\varepsilon} G[\omega;\rho], \quad (1)$$

where V is the realistic NN interaction, ρ is the nuclear matter density, ω is the starting energy, and $e(k)$ is the single-particle energy, which is a simple sum of kinetic and potential energies $U(k,\rho)$. We have used the continuous choice [7] for the potential energy,

$$U(k;\rho) = \mathrm{Re} \sum_{k' \leqslant k_F} \langle kk'|G[e(k) + e(k');\rho]|kk'\rangle_a. \quad (2)$$

The numerical details of the calculations and self-consistency requirements are described in detail [21–23]. Once the single-particle potential is calculated, one can easily calculate the binding energy per nucleon for symmetric nuclear matter of density $\rho = \frac{2}{3\pi^2}k_F^3$: k_F is the Fermi momentum of SNM,

$$\frac{E}{A} = \frac{3}{5}\frac{k_F^2}{2m} + \frac{1}{2\rho}\mathrm{Re} \sum_{k,k' \leqslant k_F} \langle kk'|G[e(k) + e(k');\rho\|kk'\rangle_a, \quad (3)$$

where the suffix a denotes antisummarization. We have used two models (UV IX and TNI) to study the effect of TBFs on the EOS.

In the present paper, we follow the methods proposed by Grangé *et al.* [8] and Lejeune *et al.* [24] in the BHF scheme to reduce the TBFs to an effective two-body force by averaging over the spin and isospin of the third particle and by folding over the appropriate relative coordinates with the product of the two-body correlation functions. The UV IX three-nucleon potential has a long-range attractive two-pion exchange part and an intermediate-range repulsive part. The final expressions for the effective two-body force are given in Appendix C of Ref. [25]. We have used the parameters for UV IX as $A = -0.0333$ and $U = 0.000\,38$ MeV with AV18 as given in Ref. [10].

The TNI model [16,17] approximates the effect of three-body forces by adding two density-dependent terms: a three-nucleon repulsive (TNR) and a three-nucleon attractive (TNA) term. The TNA is treated microscopically, whereas, the effect of the TNR is added to the calculated EOS. This effective force, expected to incorporate the TBF contributions, is added to the nuclear Hamiltonian that contains the two-body realistic interaction, and the calculations in BHF proceeds as with a two-body force. The three parameters of the TNI model were originally used [16] with UV14, and hence, we had to marginally modify them for use with AV18 to obtain the appropriate saturation properties of SNM. The parameters, as defined in Ref. [16] and as used in the present paper, are as follows: $\gamma_1 = 0.15$ fm^3, $\gamma_2 = -600$ MeV fm^6, and $\gamma_3 = 13.6$ fm^3.

To calculate the proton optical potential, we have followed the well-established method [20–23,26] by first calculating the radial effective interaction (reaction matrices), which is then folded over point proton and neutron densities in ^{40}Ca and ^{208}Pb. The relevant densities were obtained by relativistic mean-field calculations [27]. The numerically calculated real (imaginary) parts of the central $V(E,r)(W(E,r))$ and the spin orbit $V_{\mathrm{SO}}(E,r)(W_{\mathrm{SO}}(E,r))$ components of the optical potential were multiplied by scaling parameters λ and then were used in a spherical optical model code to calculate the observables,

$$U(E,r) = \lambda_R V(E,r) + i\lambda_I W(E,r) + \left(\lambda_{\mathrm{SO}}^R V_{\mathrm{SO}}(E,r) + i\lambda_{\mathrm{SO}}^I W_{\mathrm{SO}}(E,r)\right)\vec{\sigma}\cdot\vec{L},$$

where $\vec{\sigma}$ and $\vec{L}$ were the Pauli spin matrices and the orbital angular momentum of the incident proton.

The parameter λ's were adjusted to minimize χ^2/DF (where DF stands for degrees of freedom).

III. RESULTS AND DISCUSSION

Figure 1 shows our BHF results of the EOS for SNM. The figure reveals that, with only two-body internucleon potentials, the HJ underestimates, whereas, AV18, UV14, AV14, Reid93, and Nijm II overestimate the nuclear matter energy per nucleon at higher saturation densities. Thus, with only two-body forces, the nonrelativistic BHF fails to obtain either the magnitude or the density near the empirical estimates (shown as rectangles) of the saturation property, thus, our results reconfirm the Coester *et al.* band [28]. The numerical values of saturation density ρ and binding energies per nucleon $(-E/A)$, obtained in the present paper, are given in Table I.

To improve upon the predictions of the saturation property, we have used two types of TBFs along with the two-body force. Specifically, we use the Urbana IX [4] and the TNI [16,17] models of three-body forces along with UV14, AV14, and

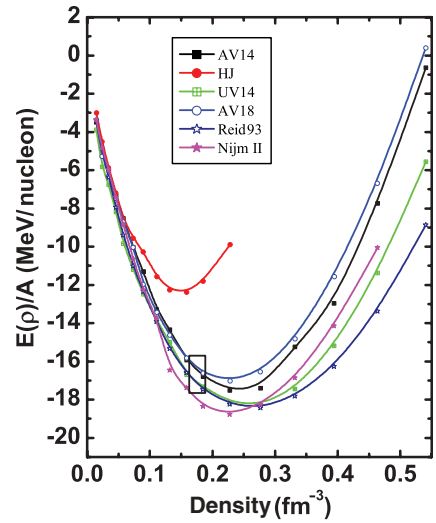

FIG. 1. (Color online) Energy per nucleon as a function of density for SNM by using only the two-body force (see text for details).

TABLE I. Saturation properties of nuclear matter obtained from different potentials.

	$\rho_0(\mathrm{fm}^{-3})$	$-E/A(\mathrm{MeV})$
Empirical values	0.17 ± 0.01	16 ± 1
HJ	0.148	12.4
Reid93	0.28	18.43
Nijm II	0.28	18.78
UV14	0.148	19.01
UV14 + UV IX	0.178	14.62
UV14 + TNI	0.157	16.6
AV14	0.228	17.52
AV14 + UV IX	0.185	16.047
AV14 + TNI	0.158	16.004
AV18	0.228	17.013
AV18 + UV IX	0.185	15.38
AV18 + TNI	0.158	16.50

AV18 internucleon potentials. The empirical estimates of the binding energy are shown as the rectangular box in Fig. 2.

The resulting EOS with TBFs are shown in Fig. 2. We note that the inclusion of TBFs yields nuclear saturation very close to the empirical estimates (see also Table I).

Microscopic calculation of the nucleon optical potential is also directly related through the folding model to the mean field in nuclear matter and, hence, the EOS. However, only two-body forces have been extensively used to calculate the nucleon optical potential for analyzing [29–32] the nucleon-nucleus scattering data except in a recent paper by Furumoto *et al.* [21]. The authors [21] have used the extended soft-core two-body force and only the phenomenological three-body force (TNI) models of Lagris and Pandharipande [16] and Friedman and Pandharipande [17]. It was found that the major effect of including the three-body forces is a reduction in the strengths of the central potential in the interior of the target. The authors [21] claim that the inclusion of TBFs improves the agreement with the experiment for the analyzing power

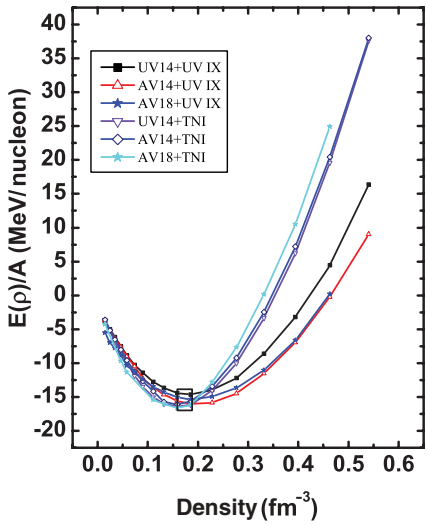

FIG. 2. (Color online) Energy per nucleon as a function of density for symmetric nuclear matter with the three-body force (UV IX and TNI models).

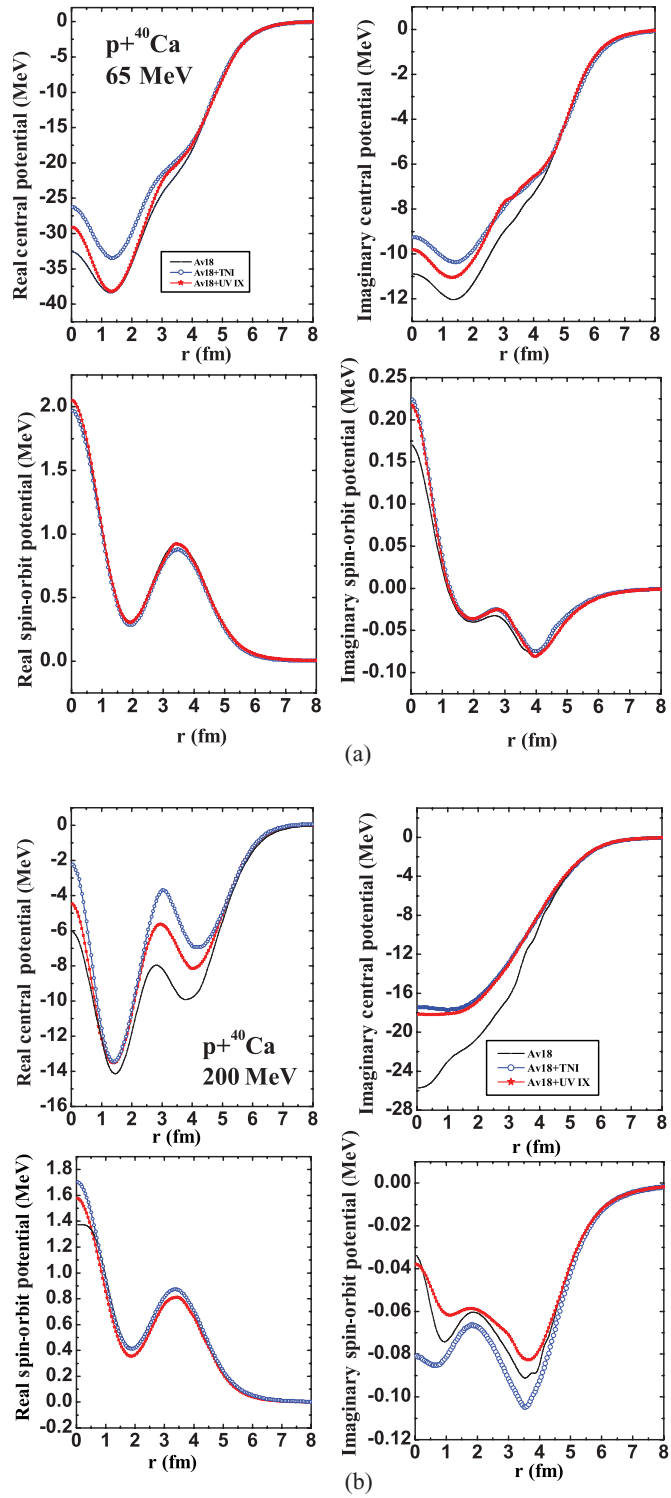

FIG. 3. (Color online) (a) Calculated real and imaginary central and spin-orbit parts of the optical potential for p-^{40}Ca at 65 MeV by using the three-body force: AV18 + UV IX (red curve with stars) and AV18 + TNI (blue curve with circles). The solid line is the result that uses AV18 (only the two-body force). (b) The same as for (a) but at 200 MeV.

data. The calculated imaginary central potential was rescaled by 0.7 to obtain agreement with the experimental data.

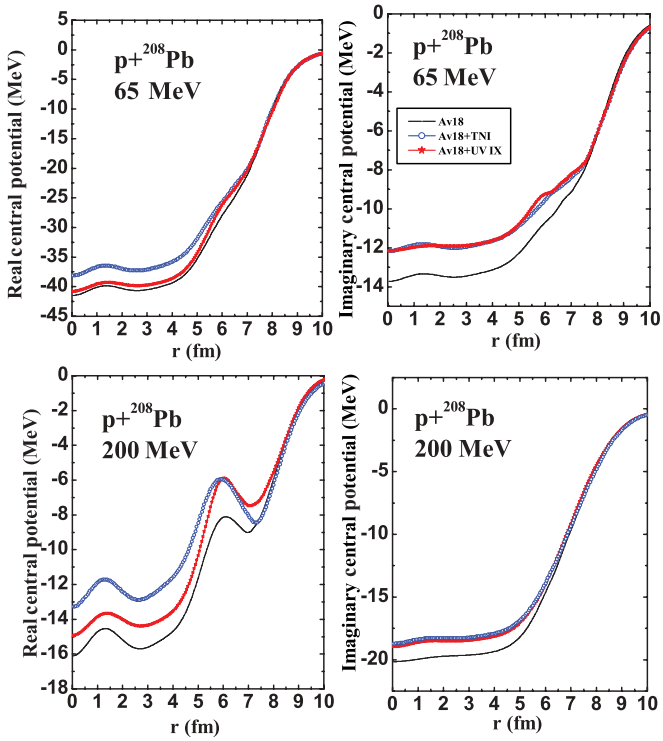

FIG. 4. (Color online) Calculated real and imaginary central parts of the optical potential for p-^{208}Pb at 65 and 200 MeV by using the three-body force: AV18 + UV IX (red curve with stars) and AV18 + TNI (blue curve with circles). The solid line is the result that uses AV18 (only the two-body force).

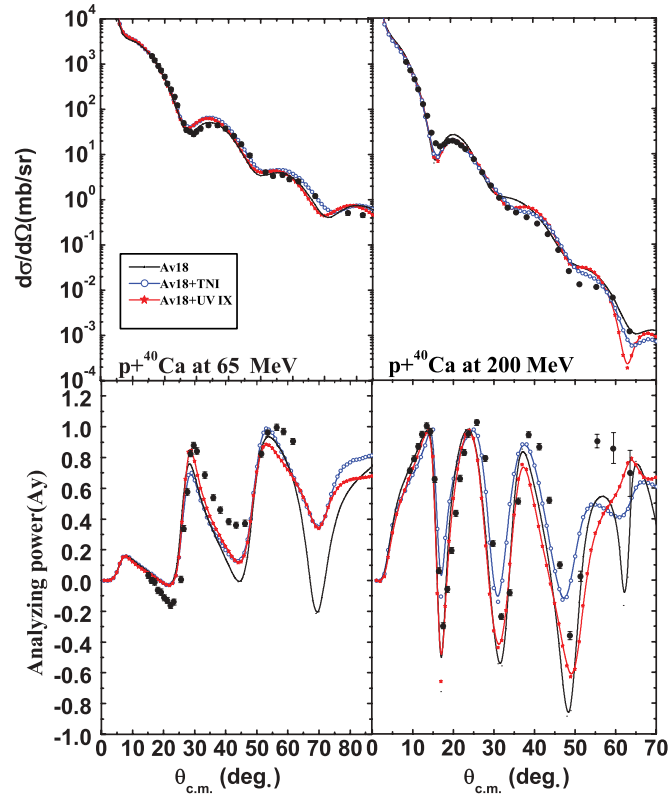

FIG. 5. (Color online) Differential cross section and analyzing power for p-^{40}Ca (left panel for 65 MeV and right panel for 200 MeV). Experimental data are taken from Refs. [33,34].

In the present paper, we report the calculation of the nucleon-nucleus optical potential by using the Argonne v18 two-nucleon interaction with both the Urbana IX [4] and the TNI [16,17] models of the three-body force. Three types of G matrices calculated by using only the two-body force AV18, AV18 + UV IX, and AV18 + TNI, are folded over the nucleon-density distributions to generate the central and spin-orbit parts of the nucleon-nucleus optical potential. Both the real and the imaginary parts of the calculated central and spin-orbit potentials for p-^{40}Ca scattering at 65 and 200 MeV are shown in Figs. 3(a) and 3(b), respectively. It is observed that the strength of the central real and imaginary potentials for p-^{40}Ca are appreciably reduced for distances $r < 5$ fm for both UV IX and TNI models of the TBFs, a result in agreement with the findings of Ref. [21]. However, there is a negligible TBF effect on the calculated spin-orbit potential. Figure 4 shows the corresponding results for p-^{208}Pb both at 65 MeV and at 200 MeV. These are similar to those for p-^{40}Ca. Since the effect of including the three-body forces on the calculated spin-orbit potential is marginal, we do not show those results for p-^{208}Pb.

TABLE II. Normalization constants obtained from a best fit at 65- (200)-MeV proton scattering from p-^{40}Ca and p-^{208}Pb. χ^2_X/DF; $X = \sigma$,pol,Q,tot represents the differential cross section, analyzing power, spin rotation, and total cross section for the experimental data analyzed.

		AV18	AV18 + UV IX	AV18 + TNI
$p + ^{40}$Ca	χ^2_σ/DF	7.41 (70.59)	7.89 (21.39)	3.61 (38.8)
	$\chi^2_{\rm pol}$/DF	53.52 (15.85)	36.15 (10.98)	25.49 (12.48)
	χ^2_Q/DF	39.76 (24.81)	26.25 (29.56)	30.98 (22.35)
	$\chi^2_{\rm tot}$/DF	32.55 (40.15)	22.79 (18.41)	19.42 (25.09)
	$\sigma_{\rm R}$ (mb)	(689.4) (536.79)	(679.7) (502.7)	(677.8) (500.7)
$p + ^{208}$Pb	χ^2_σ/DF	26.94 (37.61)	22.03 (23.4)	15.04 (21.24)
	$\chi^2_{\rm pol}$/DF	16.48 (46.45)	20.17 (24.77)	9.51 (19.8)
	χ^2_Q/DF	36.27 (13.06)	28.63 (9.03)	13.83 (7.78)
	$\chi^2_{\rm tot}$/DF	29.73 (92.39)	14.83 (64.97)	26.75 (66.96)
	$\sigma_{\rm R}$ (mb)	(2014.5) (1769.0)	(1926.2) (1684.0)	(1891.9) (1699.5)

To test the optical potential from the three G matrices (with and without three-body forces), we have used these calculated potentials to analyze the proton-scattering data from ^{40}Ca and ^{208}Pb at 65 and 200 MeV. The choice of the energies was dictated by the availability of the complete set of accurate experimental data: differential cross section, analyzing power, and spin rotation.

To obtain agreement with the experimental data, we have minimized χ^2/DF by rescaling the central part of the calculated potential. Specifically, we have to multiply the calculated imaginary potential by 0.7 (at 65 MeV) for both targets. Although, at 200 MeV, the central real (imaginary) potential had to be rescaled by 1.2 (0.7). All other λ's are kept at unity. Thus, we have varied only two parameters. This rescaling is a standard practice [29–32] in the application of the microscopic optical potential to analyze the experimental data.

Figures 5 and 6 show our results for the differential cross section and analyzing power for p-^{40}Ca and p-^{208}Pb. The black solid curve is the results using AV18 only, the blue curve with circles represents the results for AV18 + UV IX, and the red curve with stars represents AV18 + TNI interactions, respectively. Figure 7 shows the results for the spin-rotation function for both ^{40} Ca and ^{208}Pb at 65 and 200 MeV.

To demonstrate the extent of improvement, in Table II, we show the value of χ^2/DF and the scaling parameters used for the calculated potential. We note that the use of TBFs (both TNI and UV IX) gives marginally better results at both energies for targets considered in the present paper. Furthermore, the

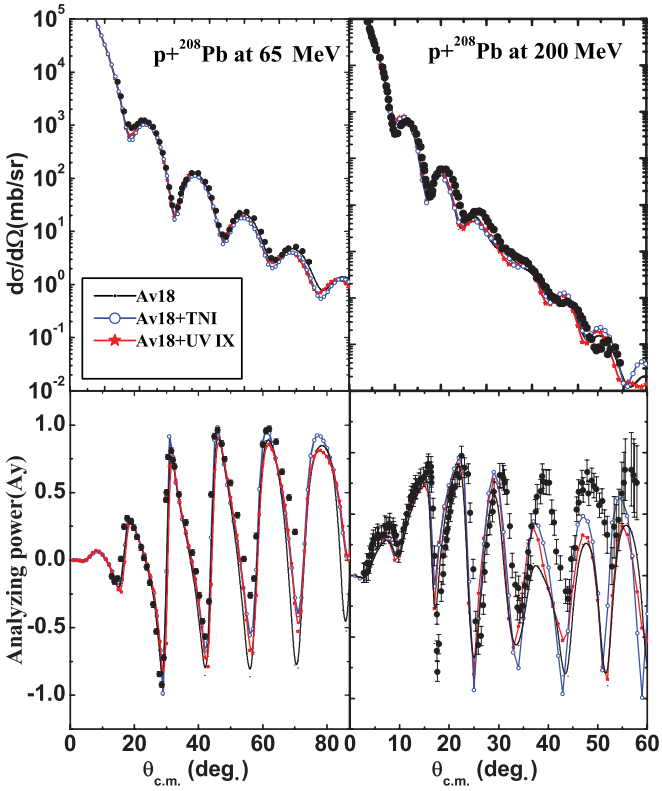

FIG. 6. (Color online) Same as for Fig. 5 but for p-^{208}Pb. Experimental data are taken from Refs. [33,34].

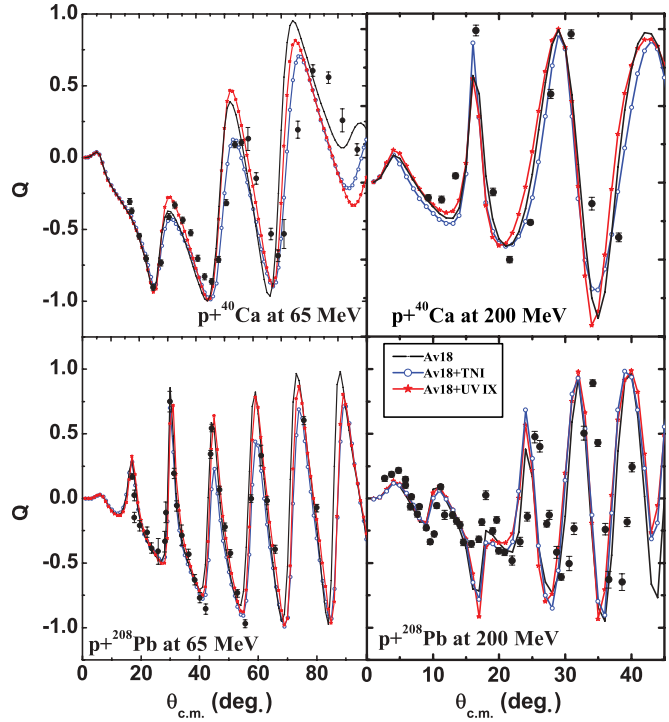

FIG. 7. (Color online) Best fit obtained for the spin-rotation function (left panel for p-^{40}Ca and ^{208}Pb, both at 65 MeV, right panel for p-^{40}Ca and ^{208}Pb, both at 200 MeV). Experimental data are taken from Refs. [33–35].

results clearly show that the quality of agreement with TBFs is much better than that obtained by using only the two-body force.

To further test the calculated potentials, in Fig. 8, we show our predictions of the proton reaction cross section for

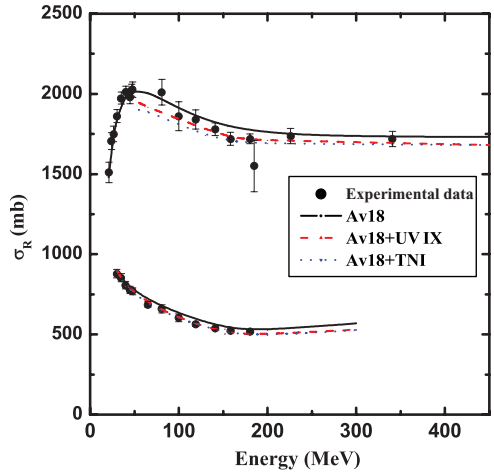

FIG. 8. (Color online) Calculated reaction cross section shown for p-^{40}Ca and p-^{208}Pb scatterings in the energy region of 30 MeV $\leqslant E \leqslant$ 300 MeV, which uses the G matrices from AV18 (black solid line), AV18 + UV IX (red dashed line), and AV18 + TNI (blue dotted line). Experimental data (solid circle) are taken from Refs. [35–39].

both ^{40}Ca and ^{208}Pb in the energy region of 30 MeV $\leqslant E \leqslant$ 300 MeV with and without three-body forces. The results show that the agreement with experiment is satisfactory.

IV. CONCLUSIONS

We have used six two internucleon potentials in BHF to calculate the EOS of SNM. Our results reconfirm the earlier findings that no two-nucleon interaction is able to reproduce the empirical saturation properties of nuclear matter. In view of this, we used two types of three-body forces with UV14, AV14, and AV18 internucleon potentials to obtain appropriate saturation properties. Furthermore, we have calculated the proton-nucleus optical potential by using AV18, which included two types of three-body forces and used it to analyze the scattering data from ^{40}Ca and ^{208}Pb at 65 and 200 MeV. The agreement with experimental data is satisfactory. Our results show that the inclusion of three-body forces reduces the strength of the central potentials in the nuclear interior, whereas, the effect on the spin-orbit part of the calculated potential is marginal.

ACKNOWLEDGMENTS

The authors are thankful to A. Bhagwat for his interest in this work. W. Haider gratefully acknowledges the financial grant from the Department of Atomic Energy (DAE), Board of Research in Nuclear Sciences (BRNS), Government of India under BRNS Project No. 2011/37P/16/BRNS. W.H. is also thankful to Dr. J. R. Rook for introducing the art of the BHF calculations. Y. K. Gambhir wishes to acknowledge the Department of Science and Technology (DST), Government of India for partial financial assistance under Project No. SR/S2/HEP-34/2009.

[1] J. P. Jeukenne, A. Lejeune, and C. Mahaux, Phys. Rep. **25**, 83 (1976); M. Baldo, *Nuclear Methods and the Nuclear Equation of State*, International Review of Nuclear Physics Vol. 8 (World Scientific, Singapore, 1999).
[2] J. Carlson, V. R. Pandharipande, and R. B. Wiringa, Nucl. Phys. A **401**, 59 (1983).
[3] A. Akmal, V. R. Pandharipande, and D. G. Ravenhall, Phys. Rev. C **58**, 1804 (1998); J. Morales, V. R. Pandharipande, and D. G. Ravenhall, *ibid.* **66**, 054308 (2002).
[4] B. S. Pudliner, V. R. Pandharipande, J. Carlson, S. C. Pieper, and R. B. Wiringa, Phys. Rev. Lett. **74**, 4396 (1995); Phys. Rev. C **56**, 1720 (1997).
[5] S. Gandolfi, A. Y. Illarionov, K. E. Schmidt, F. Pederiva, and S. Fantoni, Phys. Rev. C **79**, 054005 (2009); J. Carlson and R. Schiavilla, Rev. Mod. Phys. **70**, 743 (1998); R. B. Wiringa, S. C. Pieper, J. Carlson, and V. R. Pandharipande, Phys. Rev. C **62**, 014001 (2000); S. C. Pieper, K. Varga, and R. B. Wiringa, *ibid.* **66**, 044310 (2002); S. Gandolfi, F. Pederiva, S. Fantoni, and K. E. Schmidt, *ibid.* **73**, 044304 (2006).
[6] M. H. Kalos, Phys. Rev. **128**, 1791 (1962).
[7] H. Q. Song, M. Baldo, G. Giansiracusa, and U. Lombardo, Phys. Rev. Lett. **81**, 1584 (1998); M. Baldo, A. Fiasconaro, H. Q. Song, G. Giansiracusa, and U. Lombardo, Phys. Rev. C **65**, 017303 (2001).
[8] P. Grangé, A. Lejeune, M. Martzolff, and J.-F. Mathiot, Phys. Rev. C **40**, 1040 (1989).
[9] W. Zuo, A. Lejeune, U. Lombardo, and J.-F. Mathiot, Nucl. Phys. A **706**, 418 (2002); Eur. Phys. J. A **14**, 469 (2002).
[10] X. R. Zhou, G. F. Burgio, U. Lombardo, H.-J. Schulze, and W. Zuo, Phys. Rev. C **69**, 018801 (2004).
[11] T. Hamada and I. D. Johnston, Nucl. Phys. **34**, 382 (1962).
[12] I. E. Lagris and V. R. Pandharipande, Nucl. Phys. A **359**, 331 (1981).
[13] R. B. Wiringa, R. A. Smith, and T. L. Ainsworth, Phys. Rev. C **29**, 1207 (1984).
[14] R. B. Wiringa, V. G. J. Stoks, and R. Schiavilla, Phys. Rev. C **51**, 38 (1995).
[15] V. G. J. Stoks, R. A. M. Klomp, C. P. F. Terheggen, and J. J. deSwart, Phys. Rev. C **49**, 2950 (1994).
[16] I. E. Lagris and V. R. Pandharipande, Nucl. Phys. A **359**, 349 (1981).
[17] B. Friedman and V. R. Pandharipande, Nucl. Phys. A **361**, 502 (1981).
[18] H. A. Bethe *et al.*, Phys. Rev. **129**, 225 (1963); **138**, B804 (1965); R. Rajaraman and H. A. Bethe, Rev. Mod. Phys. **39**, 745 (1967).
[19] W. Haider, B. Sharma, and J. R. Rook, Int. J. Mod. Phys. E **14**, 807 (2005).
[20] W. Haider, A. M. Kobos, and J. R. Rook, Nucl. Phys. A **480**, 1 (1988).
[21] T. Furumoto, Y. Sakuragi, and Y. Yamamoto, Phy. Rev. C **78**, 044610 (2008).
[22] S. M. Saliem and W. Haider, J. Phys. G **28**, 1313 (2002).
[23] W. Haider, M. Sharma, Y. K. Gambhir, and S. Kailas, Phys. Rev. C **81**, 034601 (2010).
[24] A. Lejeune, P. Grange, M. Martzolff, and J. Cugnon, Nucl. Phys. A **453**, 189 (1986).
[25] M. Baldo and L. S. Ferreira, Phys. Rev. C **59**, 682 (1999).
[26] N. Yamaguchi, S. Nagata, and J. Matsuda, Prog. Theor. Phys. **70**, 459 (1983).
[27] Y. K. Gambhir, P. Ring, and A. Thimet, Ann. Phys. (NY) **198**, 132 (1990), and references therein.
[28] F. Coester, S. Cohen, B. Day, and C. M. Vincent, Phys. Rev. C **1**, 769 (1970).
[29] S. Rafi, D. Pachouri, M. Sharma, A. Bhagwat, W. Haider, and Y. K. Gambhir, Phys. Rev. C **84**, 037604 (2011).
[30] K. Amos, S. Karataglidis, and J. Dobaczewski, Phys. Rev. C **70**, 024607 (2004).
[31] S. Karataglidis, K. Amos, B. A. Brown, and P. K. Deb, Phys. Rev. C **65**, 044306 (2002), and references therein.
[32] W. Haider and M. Sharma, Int. J. Mod. Phys. E **19**, 465 (2010).
[33] H. Sakaguchi, M. Nakamura, K. Hatanaka, A. Goto, T. Noro, F. Ohtani, H. Sakamoto, H. Ogawa, and S. Kobayashi, Phys. Rev. C **26**, 944 (1982).

[34] R. A. Hutcheon *et al.*, Nucl. Phys. A **483**, 429 (1988).
[35] P. K. Deb, B. C. Clark, S. Hama, K. Amos, S. Karataglidis, and E. D. Cooper, Phys. Rev. C **72**, 014608 (2005).
[36] R. F. Carlson, At. Data Nucl. Data Tables **63**, 93 (1996).
[37] R. F. Carlson *et al.*, Phys. Rev. C **12**, 4 (1975).
[38] A. Auce *et al.*, Phys. Rev. C **71**, 064606 (2005).
[39] L. Lee and T. E. Drake, Nucl. Phys. A **492**, 607 (1989).